Resonant hyper-Raman scattering in semiconductors

A. García-Cristóbal* and A. Cantarero
Departamento de Física Aplicada, Universidad de Valencia, Burjasot, E-46100 Valencia, Spain

C. Trallero-Giner
Department of Theoretical Physics, Havana University, Vedado, 10400 Havana, Cuba

M. Cardona
Max Planck Institut für Festkörperforschung, Heisenbergstraße 1, 70569 Stuttgart, Germany
(Received 14 May 1998)

A theoretical model for resonant hyper-Raman scattering by LO phonons is developed, taking into account excitonic effects. The model is valid for energies below and above an allowed absorption edge. The matrix elements corresponding to the exciton-photon and exciton-phonon interactions are derived analytically, and their contributions to the total scattering efficiency are analyzed. The two main electron-phonon interaction mechanisms present in polar semiconductors, deformation potential, and Fröhlich interaction, are considered. It is shown that the one-phonon resonance hyper-Raman scattering mediated by the deformation potential interaction is dipole forbidden, whereas it is allowed when induced by the Fröhlich mechanism, in contrast to what happens in one-phonon Raman scattering. The calculated hyper-Raman resonance profiles show two pronounced features: an incoming resonance with the $2p$ exciton state, and a much stronger outgoing resonance related to the s excitons. The numerical values obtained illustrate the suitability of this nonlinear scattering technique for the study of the exciton structure and the exciton-phonon interaction in large-band-gap semiconductors. Our theoretical description shows a good agreement with measurements performed on ZnSe films deposited on GaAs(001) substrates. [S0163-1829(98)04139-3]

I. INTRODUCTION

In an ordinary one-phonon resonant Raman-scattering process in semiconductors, an exciton is created by means of a photon and, after the scattering by a phonon, the exciton emits a scattered photon. There exists a different kind of one-phonon Raman scattering, in which two incident photons (usually from the laser beam) contribute simultaneously to generate the electron-hole pair.[1] This nonlinear optical process is usually called hyper-Raman scattering (HRS), and the corresponding cross section is obviously proportional to the intensity of the incident light. Since its selection rules differ from those of Raman scattering and infrared absorption, HRS constitutes an additional source of spectroscopic information on the vibrational spectra of condensed media.[2,3]

Resonant Raman scattering (RRS) is characterized by a remarkable increase of the scattering efficiency when the energy of the incident or scattered photon coincides with the energy of critical points (cp's) in the band structure of solids.[4] It has been stated that an analogous resonant behavior should be expected in the HRS cross section when $2\hbar\omega_L$ or $\hbar\omega_S$ approach particular electronic transition energies (ω_L and ω_S being the frequencies of the incident and scattered photons, respectively).[5] In fact, resonance effects were already reported in $SrTiO_3$,[5] TiO_2,[6] and ZnSe.[7,8] Unfortunately, the experimental investigations on resonant hyper-Raman scattering (RHRS) are still at a very early stage. As far as the theoretical side is concerned, detailed calculations of the HRS cross section have not yet come to our knowledge. Apart from some attempt based on the polariton picture,[9] the only systematic theoretical treatment of nonlinear scattering up to date is due to Jha and Woo,[10] who deduced formal expressions for nonpolar phonon scattering, but without predicting the actual shape of the resonance profile (HRS cross section vs $2\hbar\omega_L$). In view of this lack of theoretical treatments, the present work is devoted to develop a model of RHRS, including exciton states as intermediate electronic excitations in the scattering process, which allows the study of the resonance profile around the direct optical transitions of semiconductors. It has been shown in the past that the inclusion of electron-hole interaction is essential to reproduce the Raman resonance profile around electronic transitions of semiconductors.[11,12] The results of our model are useful to predict the resonant behavior of the HRS cross section, and can be used in combination with the experimental data to obtain information on the electronic structure and electron-phonon interaction in semiconductors.

This paper is organized as follows. The proposed theoretical model for RHRS is developed in Sec. II: First we define the normalized hyper-Raman efficiency, which is the natural quantity to describe nonlinear scattering processes, and present a microscopic expression in terms of the probability amplitude for a single scattering event. In Sec. III we perform calculations of the hyper-Raman resonance profile by using the model presented in Sec. II. The role of the electron-phonon interaction is investigated. Absolute values of the normalized hyper-Raman efficiency are predicted taking ZnSe, where excitonic intermediate states are likely to be dominant, as an example. Also, the contributions of the different parts of the excitonic spectrum (discrete and continuous) to the scattering process are analyzed. In Sec. IV we compare the predictions of the model with experimental re-

sults on ZnSe. Finally, Sec. V summarizes the main conclusions of the work.

II. THEORETICAL MODEL

When comparing experimental and theoretical results of light scattering in crystals, it is convenient to express the scattered intensities in terms of the scattering efficiency $dS/d\Omega_S$, i.e., the ratio between scattered and incident power (P_S and P_L, respectively) per unit solid angle $d\Omega_S$ and unit path length (we denote the scattering length by $\mathcal{L}$) within the crystal,[4]

$$\frac{dS}{d\Omega_S}=\frac{1}{\mathcal{L}}\frac{1}{P_L}\frac{dP_S}{d\Omega_S}. \tag{1}$$

Since in the HRS process each scattered photon is emitted under simultaneous annihilation of two incident photons, the magnitude of the scattered power itself varies as the square of the laser intensity $I_L=P_L V/\mathcal{L}$ (V is the scattering volume), so that the HRS efficiency $dS_{HR}/d\Omega_S$ becomes proportional to $I_L^2/I_L=I_L$, in contrast to the intensity-independent efficiency found in ordinary Raman scattering. Accordingly, the quantity of interest is the ratio

$$\frac{d\tilde{S}_{HR}}{d\Omega_S}=\frac{1}{I_L}\frac{dS_{HR}}{d\Omega_S}=\frac{1}{V}\frac{1}{I_L^2}\frac{dP_S}{d\Omega_S}, \tag{2}$$

usually referred to as *normalized hyper-Raman efficiency* (HR efficiency from here on), and expressed in units of $\mathrm{cm(MW\,sr)}^{-1}$.

From a microscopic point of view the HRS process is described as follows: two photons of wave vector $\vec{\kappa}_L$, polarization $\vec{e}_L$, and frequency ω_L scatter an optical phonon of wave vector $\vec{q}$ and frequency ω_ν (ν indicates the optical branch), whereby a photon of wave vector $\vec{\kappa}_S$, polarization $\vec{e}_S$, and frequency ω_S is emitted (see Fig. 1). The HR efficiency can be shown to be related to the scattering amplitude W_{FI} by[4,11,12]

$$\frac{d\tilde{S}_{HR}}{d\Omega_S}=\frac{V^2}{(2\pi)^2}\omega_L\omega_S^3\frac{\eta_L^2\eta_S^3}{c^5}\frac{1}{(\hbar\omega_L)^3}(N_\nu+1)\sum_{\vec{q}}|W_{FI}|^2, \tag{3}$$

with the conservation of energy $\hbar\omega_S=2\hbar\omega_L-\hbar\omega_\nu$ implicitly understood. η_L (η_S) is the refractive index of the incident (scattered) radiation, c is the speed of light in vacuum, and N_ν represents the Bose-Einstein phonon occupation factor (only Stokes scattering is considered in this work). In both the initial and final states of the scattering process, denoted $|I\rangle$ and $|F\rangle$, respectively, the electronic system of the semiconductor is assumed to be in its ground state.

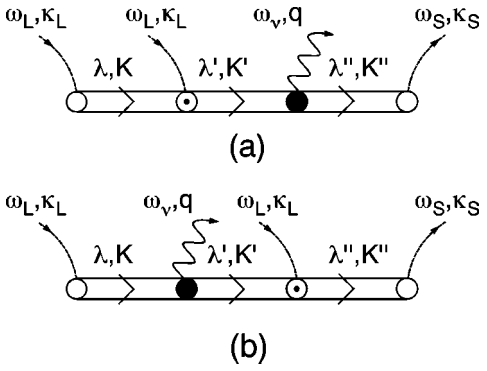

FIG. 1. Feynman diagrams which give the main contribution to resonant hyper-Raman scattering.

In resonance conditions, when $2\hbar\omega_L$ and/or $\hbar\omega_S$ are close to electronic excitation energies, the main contribution to W_{FI} is expected to follow from the process schematically shown in Fig. 1(a). In a first step, the absorption of a photon by the crystal creates an exciton in the state characterized by $(\lambda,\vec{K})$ (λ represents the exciton inner quantum numbers, and $\vec{K}$ its center-of-mass wave vector). The absorption of a second photon scatters the exciton to the intermediate state $(\lambda',\vec{K}')$. Next, an excitonic transition to the state $(\lambda'',\vec{K}'')$ takes place after the creation of an optical phonon, and finally we have the exciton annihilation with the emission of a photon. Other processes which can contribute to HRS can be obtained by permuting the interaction vertices in the diagram of Fig. 1(a). Their contributions are, in general, nonresonant, and thus can be neglected in the study of RHRS. The only additional diagram which could *a priori* be important is the one constructed by exchanging second and third vertices in Fig. 1(a) [see Fig. 1(b)]. Nevertheless, our unpublished calculations show that the corresponding amplitude is almost two orders of magnitude smaller than that associated with the process in Fig. 1(a), which will therefore be the only one included in our model. The scattering amplitude appearing in Eq. (3) is then represented by

$$W_{FI}=\sum_{\lambda'',\vec{K}''}\sum_{\lambda',\vec{K}'}\sum_{\lambda,\vec{K}}\frac{\langle F|\hat{H}_{e\text{-}R}|\lambda'',\vec{K}''\rangle\langle\lambda'',\vec{K}''|\hat{H}_{e\text{-}L}|\lambda',\vec{K}'\rangle\langle\lambda',\vec{K}'|\hat{H}_{e\text{-}R}|\lambda,\vec{K}\rangle\langle\lambda,\vec{K}|\hat{H}_{e\text{-}R}|I\rangle}{[\hbar\omega_S-E_{\lambda''}(\vec{K}'')+i\Gamma_{\lambda''}(\vec{K}'')][2\hbar\omega_L-E_{\lambda'}(\vec{K}')+i\Gamma_{\lambda'}(\vec{K}')][\hbar\omega_L-E_\lambda(\vec{K})+i\Gamma_\lambda(\vec{K})]}, \tag{4}$$

where $\hat{H}_{e\text{-}L}$ and $\hat{H}_{e\text{-}R}$ are the Hamiltonian operators for the interaction of the electronic system with the lattice vibrations and the radiation field, respectively. $|\lambda,\vec{K}\rangle$ are exciton states with energy $E_\lambda(\vec{K})$ and lifetime broadening $\Gamma_\lambda(\vec{K})$. These states are treated here in the framework of the Wannier-Mott exciton model.[11] When the relative electron-hole (e-h) motion is expressed in spherical coordinates, λ represents the set of quantum numbers $\lambda\equiv(\xi,l,m)$:[11] ξ can be either n, for the discrete spectrum, or k, for the continuous spectrum [band indices (v,c) are also implicit in the notation]. The exciton energy $E_\lambda(\vec{K})\equiv E_\xi(\vec{K})$ is given by

$$E_\xi(\vec{K})=E_g+\frac{\hbar^2\vec{K}^2}{2M}+\Delta E_\xi, \tag{5}$$

where $M=m_c+m_v$ is the exciton mass (m_c and m_v are the electron and hole masses), and ΔE_ξ the energy associated to the relative motion, which can be written as

$$\Delta E_\xi = \begin{cases} \Delta E_n = -\dfrac{R}{n^2} & \text{if} \quad \xi = n \\ \Delta E_k = Rk^2 & \text{if} \quad \xi = k. \end{cases} \tag{6}$$

R is the exciton Rydberg and $k=k_{\rm in}a$, where $\vec{k}_{\rm in}$ is the wave vector for the relative (internal) motion and a the exciton Bohr radius.

The matrix element $\langle \lambda,\vec{K}|\hat{H}_{e\text{-}R}|I\rangle$ for allowed optical transitions is given, in the electric dipole approximation ($\vec{\kappa}\simeq 0$), by[13]

$$\langle \lambda,\vec{K}|\hat{H}_{e\text{-}R}|I\rangle = \delta_{\vec{K},\vec{\kappa}_L}\frac{e}{m_0}\sqrt{\frac{2\pi\hbar}{\omega_L\eta_L^2}}(\vec{e}_L\cdot\vec{p}_{cv})\varphi_\lambda(0)^*, \tag{7}$$

$\varphi_\lambda(\vec{r})$ being the exciton envelope function for the relative motion, $\vec{p}_{cv}$ the interband momentum matrix element between valence and conduction Bloch functions at the Γ point, and m_0 the free-electron mass. Of course, $\langle F|\hat{H}_{e\text{-}R}|\lambda'',\vec{K}''\rangle$ is obtained after complex conjugation of Eq. (7), and a change of subscripts $L\to S$.

The matrix element $\langle \lambda',\vec{K}'|\hat{H}_{e\text{-}R}|\lambda,\vec{K}\rangle$ represents the probability amplitude for the scattering of the exciton between states $(\lambda,\vec{K})$ and $(\lambda',\vec{K}')$, induced by the interaction Hamiltonian $\hat{H}_{e\text{-}R}$. Several possibilities arise.[14] There may be *interband excitonic transitions*, accompanied by scattering of the electron or hole between different bands, and there are also *intraband excitonic transitions* in which the electron and hole remain in the same band, and only the exciton envelope function is affected by the interaction with the radiation field. Whether the main contribution to the scattering involves intraband or interband transitions, or any other path, depends in general upon the parameters of the material and the laser energy employed. We feel that when $2\hbar\omega_L$ is around the E_0 gap of II-VI and III-V semiconductors, the remainder of bands are sufficiently far in energy so that their contribution through interband transitions can be neglected, thus in this work only intraband transitions are considered. In this case the explicit expression for the matrix element is, in the dipole approximation,[14]

$$\langle \lambda',\vec{K}'|\hat{H}_{e\text{-}R}|\lambda,\vec{K}\rangle = \delta_{\vec{\kappa}_L,\vec{K}'-\vec{K}}\frac{e}{\mu}\sqrt{\frac{2\pi\hbar}{\omega_L\eta_L^2}}\frac{1}{\sqrt{V}}P_{\lambda\to\lambda'}(\vec{e}_L), \tag{8}$$

which is the result usually employed in the calculations of two-photon absorption.[15] In Eq. (8), $\mu=m_v m_c/M$ is the exciton reduced mass, and

$$P_{\lambda\to\lambda'}(\vec{e}) = \vec{e}\cdot\int d^3\vec{r}\,\varphi_{\lambda'}(\vec{r})^*(-i\hbar\vec{\nabla})\varphi_\lambda(\vec{r}). \tag{9}$$

The explicit expressions for the above integrals are presented in the Appendix, where it is shown that for transitions between exciton states with $m=0$ (the only ones which participate in the process studied here), the interaction with the photon field induces a change of a unity in the orbital quantum number l. Since we are treating the case of an allowed absorption edge, only $l=0$ excitons participate in the first and last steps of the scattering process of Fig. 1(a), and therefore the exciton state participating in the second step must be necessarily of p-type ($l=1$).

In Eq. (4), $\langle \lambda',\vec{K}'|\hat{H}_{e\text{-}L}|\lambda,\vec{K}\rangle$ is the matrix element of the electron-phonon interaction between two exciton states, belonging in general to different valence bands v and v' (masses m_v and $m_{v'}$) and conduction bands c and c' (masses m_c and $m_{c'}$). It has the form[16,17]

$$\langle \lambda',\vec{K}'|\hat{H}_{e\text{-}L}|\lambda,\vec{K}\rangle = \delta_{\vec{K}'+\vec{q},\vec{K}}[\mathcal{V}_{c',c}(\vec{q})\delta_{v,v'}I_{\lambda\to\lambda'}(-\vec{q}_e) - \delta_{c',c}\mathcal{V}_{v,v'}(\vec{q})I_{\lambda\to\lambda'}(\vec{q}_h)], \tag{10}$$

where the first term corresponds to scattering of the electron and the second term to scattering of the hole. $\mathcal{V}_{s's}\equiv\langle s'|\mathcal{V}|s\rangle$ is the matrix element of the electron-phonon interaction potential $\mathcal{V}$ (in $\vec{q}$ space) between the Γ-point Bloch states $|s\rangle$ and $|s'\rangle$. The vectors $\vec{q}_e$ and $\vec{q}_h$ are

$$\vec{q}_e = \frac{m_v}{m_c+m_v}\vec{K} - \frac{m_{v'}}{m_{c'}+m_{v'}}\vec{K}', \tag{11a}$$

$$\vec{q}_h = \frac{m_c}{m_c+m_v}\vec{K} - \frac{m_{c'}}{m_{c'}+m_{v'}}\vec{K}', \tag{11b}$$

and

$$I_{\lambda\to\lambda'}(\vec{q}) = \int d^3\vec{r}\,\varphi_{\lambda'}(\vec{r})^* e^{i\vec{q}\cdot\vec{r}}\varphi_\lambda(\vec{r}). \tag{12}$$

An exhaustive study of the integrals of Eq. (12) was performed in Refs. 11 and 12, and we refer to them for further details.

By using Eqs. (7), (8), and (10) we find that W_{FI} is proportional to $\delta_{2\vec{\kappa}_L+\vec{q},\vec{\kappa}_S}$ (conservation of wave vector in the global scattering process), and the sum $\Sigma_{\vec{q}}$ in Eq. (3) drops out. The resulting expression for the amplitude is

$$W_{FI} = r_e c^2\frac{1}{\sqrt{V}}\frac{e}{m_0}\left(\frac{2\pi\hbar}{\omega_L\eta_L^2}\right)\sqrt{\frac{2\pi\hbar}{\omega_S\eta_S^2}}\frac{(\vec{e}_L\cdot\vec{p}_{cv})(\vec{e}_S^{\,*}\cdot\vec{p}_{v'c'})}{m_0}\sum_{\xi'}\frac{1}{2\hbar\omega_L - E_g - \Delta E_{\xi'} + i\Gamma_{\xi'}}\left\{\frac{m_0}{\mu}\sum_\xi\frac{\varphi_{\xi,0}(0)^*\ P_{\xi,0\to\xi',1}(\vec{e}_L)}{\hbar\omega_L - E_g - \Delta E_\xi + i\Gamma_\xi}\right\}$$

$$\times\left\{\sum_{\xi''}\frac{[\mathcal{V}_{c',c}(\vec{q})\delta_{v,v'}I_{\xi',1\to\xi'',0}(-\vec{q}_e) - \delta_{c',c}\mathcal{V}_{v,v'}(\vec{q})I_{\xi',1\to\xi'',0}(\vec{q}_h)]\ \ \varphi_{\xi'',0}(0)}{\hbar\omega_S - E_g' - \Delta E_{\xi''} + i\Gamma_{\xi''}}\right\}, \tag{13}$$

where $r_e = e^2/m_0 c^2$ is the classical (Thomson) electron radius. In the above expression, although we have neglected the wave-vector dependences in the denominators, we have retained the small but finite value of $\vec{q}_e$ and $\vec{q}_h$ in the exciton-phonon matrix element.

It is worth noticing that $P_{\xi,0\to\xi',1}(\vec{e})$ is proportional to the z component of the photon polarization vector, e_z (see the Appendix). In our calculations the z axis (taken to be the quantization axis of the exciton angular momentum) lies along the phonon wave vector $\vec{q}$, and therefore we have $P_{\xi',0\to\xi,l}(\vec{e}_L)\propto \vec{e}_L\cdot\hat{\vec{q}}$ ($\hat{\vec{q}}$ is a unit vector along $\vec{q}$). This means that the mechanism we have proposed to describe HRS is only effective if the polarization vector of the incident radiation lies in the scattering plane determined by the wave vectors of the incident and scattered photons. As a trivial consequence of this fact, the HRS process displayed in Fig. 1 should be forbidden in an exact backward scattering configuration, with $\vec{\kappa}_S$ antiparallel to $\vec{\kappa}_L$.

III. RESONANT HYPER-RAMAN EFFICIENCY

We further proceed with the application of Eq. (13) to calculate the HR resonance profile around the E_0 and $E_0+\Delta_0$ gaps of zinc-blende-type semiconductors. We will assume three independent valence bands [heavy holes (hh), light holes (lh), and spin-orbit split-off holes (so)] and only the Γ_6 conduction band of s symmetry.

A. Role of exciton-phonon interaction

Let us analyze RHRS mediated by the two kinds of electron–optical-phonon interaction present in zinc-blende compounds, namely, deformation potential and Fröhlich interaction. The deformation potential interaction by optical phonons cannot couple Γ_6 conduction-band Bloch states in zinc-blende semiconductors.[18] Thus in this case the scattering by the phonon involves only the hole part of the exciton, and the matrix element (10) reduces to[19]

$$\langle\lambda',\vec{K}'|\hat{H}_{e\text{-}L}|\lambda,\vec{K}\rangle = -\delta_{\vec{K}'+\vec{q},\vec{K}}\delta_{c',c}\frac{\overline{u_0}\sqrt{3}}{2a_0}\langle v|\hat{D}_h|v'\rangle I_{\lambda\to\lambda'}(\vec{q}_h), \tag{14}$$

where $\overline{u_0}$ is the phonon displacement, a_0 the lattice constant, and $\hat{D}_h$ the deformation potential matrix as defined by Bir and Pikus.[18]

As explicitly shown in Eq. (13), the phonon emission is accompanied by excitonic transitions between states with diferent angular momentum l. The integral $I_{\xi',1\to\xi'',0}(\vec{q}_h)$ vanishes in the dipole approximation ($\vec{\kappa}_{L,S}\to 0$), due to the orthogonality of envelope functions with different l [see Eq. (12) and Ref. 11]. Therefore, we conclude that RHRS mediated by the deformation potential interaction is dipole-forbidden.

When the hyper-Raman process is induced by the Fröhlich interaction, on the contrary, the symmetry of the electron-phonon coupling requires transitions between states in the same band [$\vec{q}_e=(m_v/M)\vec{q}$ and $\vec{q}_h=(m_c/M)\vec{q}$], and the matrix element (10) can be written as

$$\langle\lambda',\vec{K}'|\hat{H}_{e\text{-}L}|\lambda,\vec{K}\rangle = \delta_{\vec{K}'+\vec{q},\vec{K}}\delta_{c',c}\delta_{v,v'}\frac{1}{\sqrt{V}}\frac{C_F^*}{q}[I_{\lambda\to\lambda'}(-\vec{q}_e)-I_{\lambda\to\lambda'}(\vec{q}_h)], \tag{15}$$

where C_F is the Fröhlich coupling constant,

$$C_F = -i\sqrt{2\pi\hbar\omega_{\rm LO}e^2\left(\frac{1}{\varepsilon_\infty}-\frac{1}{\varepsilon_0}\right)}, \tag{16}$$

ε_∞ and ε_0 being the optical and static dielectric constants, respectively. Taking the limit $q\to 0$, the exciton-phonon coupling yields the nonvanishing result:

$$\frac{1}{q}[I_{\xi,0\to\xi',1}(-\vec{q}_e)-I_{\xi,0\to\xi',1}(\vec{q}_h)]\overset{q\to 0}{\to}\frac{1}{3}\frac{m_v-m_c}{m_v+m_c}\mathcal{R}_{\xi,0\to\xi',1}, \tag{17}$$

where the function $\mathcal{R}_{\xi,0\to\xi',1}$ is given in the Appendix.

In conclusion, the RHRS considered here is dipole-forbidden when the electron-phonon interaction involved is deformation potential, whereas it is dipole-allowed when it is induced by Fröhlich interaction. This is in contrast with first-order RRS, for which the opposite selection rules hold.[19,20] The reason for this is that the introduction of a new photon changes the parity of the accessible intermediate electronic states from s to p, a well-known situation in two-photon spectroscopy.[15] On the basis of the above argument one does not expect to see effects derived from deformation potential interaction in RHRS. In Ref. 21 it was experimentally shown that the contribution of Fröhlich (electro-optic) interaction to the HRS by LO phonons in ZnS, ZnSe, and CdS is 1–2 orders of magnitude larger than the intensities of HRS by TO phonons (induced necessarily by deformation potential interaction). Thus only the dipole-allowed Fröhlich-interaction-induced process will be considered from here on.

B. Hyper-Raman resonance profile

By using Eqs. (3), (13), and (15), the HR efficiency can be expressed as

$$\frac{d\tilde{S}_{HR}}{d\Omega_S} = T_0(N_{\rm LO}+1)|C_F|^2\left|\frac{1}{q}\sum_v \mathcal{C}(v)\mathcal{W}(v)\right|^2, \tag{18}$$

where

$$T_0 = r_e^2\left(\frac{\omega_S}{\omega_L}\right)^2\frac{\eta_S}{\eta_L}\left(\frac{P^2}{m_0}\right)^2\frac{\eta_L}{c}\frac{1}{\hbar\omega_L}\left(\frac{e}{m_0}\sqrt{\frac{2\pi\hbar}{\omega_L\eta_L^2}}\right)^2, \tag{19}$$

and $P=|\langle s|p_x|x\rangle|$. In Eq. (18) the sum runs over heavy, light, and split-off exciton states ($v=v_{\rm hh},v_{\rm lh},v_{\rm so}$). The function $\mathcal{W}(v)$ is given by

$$\mathcal{W}(v)=\sum_{\xi'}\frac{1}{2\hbar\omega_L-E_g-\Delta E_{\xi'}+i\Gamma_{\xi'}}\left\{\frac{m_0}{\mu}\sum_{\xi}\frac{\varphi_{\xi,0}(0)^*P_{\xi,0\to\xi',1}(\vec{e}_L)}{\hbar\omega_L-E_g-\Delta E_{\xi}+i\Gamma_{\xi}}\right\}\left\{\sum_{\xi''}\frac{[I_{\xi'',0\to\xi',1}(q_e)+I_{\xi'',0\to\xi',1}(q_h)]\varphi_{\xi'',0}(0)}{\hbar\omega_S-E_g-\Delta E_{\xi''}+i\Gamma_{\xi''}}\right\}, \tag{20}$$

with the weight factor $\mathcal{C}(v)$ equal to

$$\mathcal{C}(v)=\frac{1}{P^2}\langle c|\vec{e}_L\cdot\vec{p}|v\rangle\langle v|\vec{e}_S^{\,*}\cdot\vec{p}\,|c\rangle. \tag{21}$$

In order to write Eq. (20) we have used some properties of the integrals (12), which can be found in the Appendix of Ref. 11.

In the RHRS experiments discussed below, $2\hbar\omega_L$ is in, or slightly above, resonance with an interband electronic transition of the material. Under these conditions, if E_g is sufficiently large as compared to the Rydberg energy R and the LO-phonon energy $\hbar\omega_{\mathrm{LO}}$, the second denominator in Eq. (20) is very far from resonance, and we can assume that $|\hbar\omega_L-E_g|\gg\Delta E_\xi$ for the exciton states ξ relevant to the resonance behavior. By taking into account the closure relation

$$\sum_{\lambda}\varphi_\lambda(0)\varphi_\lambda(\vec{r})^*=\delta(\vec{r}),$$

it is easy to verify that

$$\mathcal{W}(v)\simeq-\frac{\delta^2}{R}\sum_{\xi'}\frac{m_0}{\mu}\frac{(-i\hbar)\vec{e}_L\cdot\vec{\nabla}\varphi_{\xi',1}(\vec{r})|_{\vec{r}=0}}{2\hbar\omega_L-E_g-\Delta E_{\xi'}+i\Gamma_{\xi'}}\sum_{\xi''}\frac{[I_{\xi'',0\to\xi',1}(q_e)+I_{\xi'',0\to\xi',1}(q_h)]\varphi_{\xi'',0}(0)}{\hbar\omega_S-E_g-\Delta E_{\xi''}+i\Gamma_{\xi''}}, \tag{22}$$

where $\delta^2=R/(E_g-\hbar\omega_L)$. This approximate result depends on the derivative of the exciton envelope function at $\vec{r}=0$, $\vec{\nabla}\varphi_{\xi',1}(\vec{r})|_{\vec{r}=0}$. This feature, first recognized in the calculation of two-photon absorption,[15] makes the two-photon transition arising at the first steps of the scattering process resemble a one-photon forbidden transition, known to bring the electronic system to a p- ($l=1$) exciton state. Thus expression (22) is formally similar to that appearing in first-order RRS (for a photon of energy $2\hbar\omega_L$),[20] except for the presence of the factor $\vec{e}_L\cdot\vec{\nabla}\varphi_{\xi',0}(\vec{r})|_{\vec{r}=0}$ instead of $\varphi_{\xi',0}(0)$. Otherwise stated, the RHRS process is *equivalent* to a RRS process in which the first interband transition, corresponding to the absorption of a photon $2\hbar\omega_L$, is dipole forbidden (p-exciton states are responsible for the incoming resonance), whereas the last one, corresponding to the emission of the scattered photon $\hbar\omega_S$, is allowed (s-exciton states are responsible for the outgoing resonance). This possibility of probing s- and p-exciton states in the same experiment is one of our predicted and not yet demonstrated advantages of RHRS experiments. Even if only the incoming resonance is studied, the technique of RHRS is potentially advantageous to study electronic states of different symmetry to those participating in RRS.

In order to illustrate the particular features of the resonant behavior of HRS, we have performed calculations of the HR efficiency in a realistic case. We have chosen the parameters of ZnSe (see Table I), a material where excitonic effects are clearly observed in RRS.[11] Figure 2 displays the corresponding HR resonance profile for $2\hbar\omega_L$ around the E_0 gap, as obtained by applying Eqs. (18)–(20). For reasons which will become clear in Sec. IV, only the contribution of the light-hole valence band v_{lh} has been considered here. In the sum over intermediate states of Eq. (20) we have included states from the discrete spectrum with a quantum number up to $n=4$, whereas the contribution of the continuous spectrum has been fully taken into account (except for continuum-continuum transitions, which have been neglected since we are studying here a one-phonon process[19,20]). The lifetime broadening of the continuum states is taken to be independent of k and equal to Γ_c. The $n=1$ and 2 exciton states have been assigned a unique lifetime broadening Γ_1, and for the remainder of the states we use a value Γ_n obtained from

TABLE I. Numerical values of the ZnSe parameters used for the calculation of the HR efficiencies displayed in Figs. 2–4.

Parameters	Values
E_0 (lh)	2.82060 eV [a]
E_0 (hh)	2.822776 eV [a]
$\hbar\omega_{\mathrm{LO}}$	31.75 meV [b]
m_c	0.15 m_0 [b]
m_{hh}	0.78 m_0 [b]
m_{lh}	0.14 m_0 [b]
$\tilde{m}_{\mathrm{h}}$	0.24 m_0 [c]
R	19 meV [b]
$\tilde{a}$	46.7 Å [d]
P^2/m_0	9.4 eV [e]
ε_0	9 [b]
ε_∞	5.5 [b]
$\lvert C_F\rvert$	4.5×10^{-5} eV cm$^{1/2}$ [f]

[a] Reference 27.
[b] Reference 29.
[c] $1/\tilde{m}_h=\frac{1}{2}[(1/m_{\mathrm{hh}})+(1/m_{\mathrm{lh}})]$.
[d] $\tilde{a}=\sqrt{(R_H/R)[(1/m_e)+(1/\tilde{m}_h)]}\,a_H$, where R_H and a_H are the Rydberg and Bohr radius of the hydrogen atom, respectively.
[e] $P\sim2\pi\hbar/a_0$.
[f] See Eq. (16).

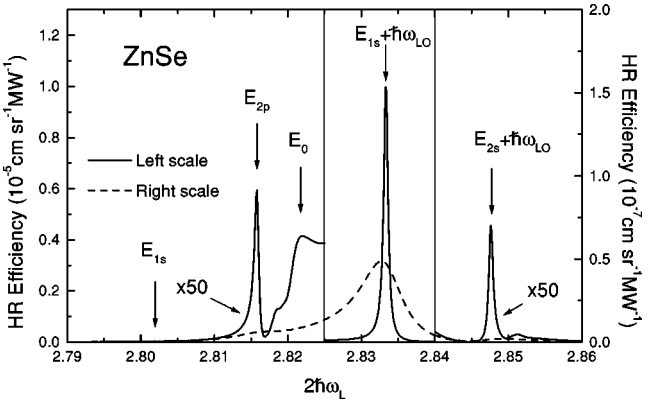

FIG. 2. Dependence of the HR efficiency on $2\hbar\omega_L$. The parameters employed are those of ZnSe, and can be found in Table I (only the contribution due to the lh exciton is shown in the figure). The solid (dashed) line has been obtained using $\Gamma_1=0.35$ meV and $\Gamma_c=1$ meV ($\Gamma_1=3.5$ meV and $\Gamma_c=10$ meV).

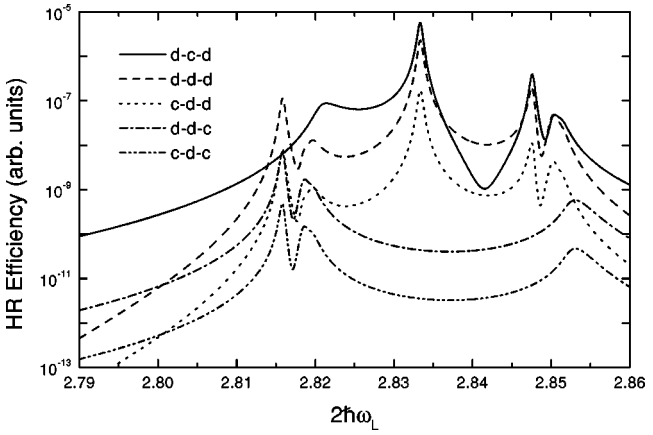

FIG. 3. Contribution of the different intermediate excitonic transitions to the HR efficiency. The parameters employed in the calculations are the same as for the solid lines in Fig. 2.

interpolation between Γ_1 and Γ_c. The continuous lines in Fig. 2 represent the results obtained with the values $\Gamma_1=0.35$ meV and $\Gamma_c=1$ meV, reasonable for samples of high purity and at low temperature. The dashed line shows the HR efficiency obtained by using larger values, $\Gamma_1=3.5$ meV and $\Gamma_c=10$ meV. Several sharp features can be distinguished in the small broadening resonance profile: as advanced above, the incoming resonance takes place when $2\hbar\omega_L$ matches the energy of the $2p$ exciton state, $E_{2p}=E_0-R/4$. Also, a small shoulder is apparent when twice the photon energy is in resonance with the band-to-band transitions, $2\hbar\omega_L\simeq E_0$. There is no incoming resonance at $2\hbar\omega_L=E_{1s}=E_0-R$, since after the absorption of the two photons the exciton cannot have $l=0$, but we can observe a strong enhancement of the efficiency when $\hbar\omega_S=E_{1s}$ (outgoing resonance) and even for $\hbar\omega_S=E_{2s}$. It is noticeable that, as compared to the off- (below-)resonance results, the efficiency is increased by a factor ~ 100 when $2\hbar\omega_L=E_{2p}$, and up to 10^4 for $\hbar\omega_S=E_{1s}$, thus reaching absolute values of the HR efficiency between 10^{-7} and 10^{-5} cm(MW sr)$^{-1}$. These values imply, for an incident laser intensity of 100 MW/cm^2, and scattering efficiencies in the range $10^{-4}-10^{-2}$ sr^{-1} cm^{-1}, which are comparable with the Raman efficiencies obtained under resonance conditions in several zinc-blende-type semiconductors.[11,12] These predicted values show the feasibility of the RHRS experiments as far as the intensity of the scattered signal is concerned (at least for laser energies such that $\hbar\omega_S<E_{1s}$, because for larger energies the scattered signal begins to experience a strong reabsorption, which may hinder its detection). Nevertheless, from the comparison between the results in solid and dashed lines of Fig. 2(a), it is evident that as the broadening of the exciton states is increased (even for values below 10 meV), the different features of the resonance profile rapidly smear out and become less defined, and therefore they are unlikely to be resolved in experiments performed at high temperatures and/or on low-quality samples. Furthermore, the signal will be obviously weaker under these circumstances; for the values of the broadening used in this example, a decrease of two orders of magnitude in the HR efficiency is observed (the dashed line has been enhanced by a factor of 100; see right scale). The calculations of the HR efficiency for exciton-phonon interaction via deformation potential (not presented here) give results four orders of magnitude smaller than those shown in Fig. 2, as is expected from the dipole-forbidden character of that mechanism.

It is also interesting to analyze the relative importance of the different sequences of exciton intermediate states which can arise from the sums in Eq. (20). We have calculated separately the contributions to the efficiency due to discrete $\rightarrow$discrete$\rightarrow$discrete ($d\rightarrow d\rightarrow d$) discrete$\rightarrow$discrete$\rightarrow$continuous ($d\rightarrow d\rightarrow c$), discrete$\rightarrow$continuous$\rightarrow$discrete ($d\rightarrow c\rightarrow d$), continuous$\rightarrow$discrete$\rightarrow$discrete ($c\rightarrow d\rightarrow d$), and continuous$\rightarrow$discrete$\rightarrow$continuous ($c\rightarrow d\rightarrow c$) transitions, and their square absolute values are represented in Fig. 3. We can see that the fundamental contributions to the HR efficiency arise from the combination of $d\rightarrow c\rightarrow d$ and $d\rightarrow d\rightarrow d$ excitonic transitions, the remainder being at least a factor of 10 smaller. Of course, the total efficiency is constructed by coherent superposition of the corresponding amplitudes, and interference effects are always present; moreover, the sequences containing continuous$\rightarrow$continuous excitonic transitions are absent from our calculations. Nevertheless, the results shown in Fig. 3 are illustrative in the sense that they display clearly that the more important paths for the scattering process are those through the exciton states which allow the second and third denominators of Eq. (4) to vanish.[11] We also have to consider that sequences containing continuous states present a somewhat reduced contribution, due to the larger broadening of these states. On these grounds it can be understood why the $d\rightarrow d\rightarrow d$ transitions dominate the resonance profile in the incoming resonance region, while the $d\rightarrow c\rightarrow d$ ones become of comparable importance for $2\hbar\omega_L>E_0$, and exhibit a (slightly) larger contribution in the outgoing region.

IV. COMPARISON WITH EXPERIMENT

Despite the potential advantages of this nonlinear spectroscopic technique, experimental studies of RHRS are still rare in the literature.[5–8] In particular, the only reported measurements on zinc-blende semiconductors, to our knowledge, are those of Refs. 7 and 8, carried out on ZnSe thin films. In this

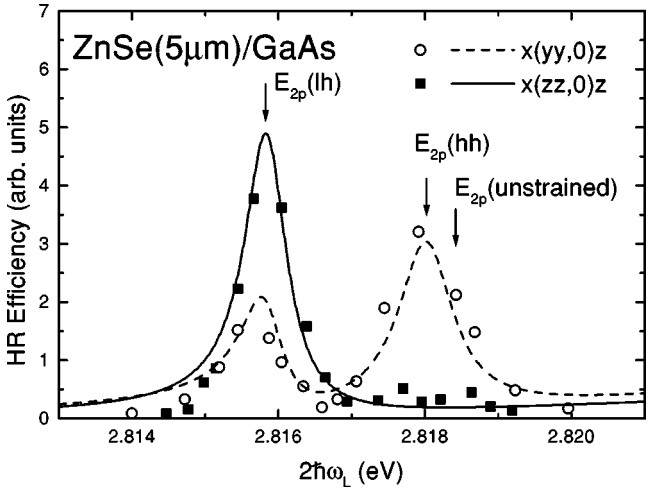

FIG. 4. Hyper-Raman resonance profile around the critical point E_0 of ZnSe: experimental data are given by the black circles [$x(yy,0)z$ scattering geometry] and squares [$x(zz,0)z$] (Ref. 7), and theoretical calculations by the solid and dashed lines (the parameters employed are listed in Table I).

section we compare those experimental data with the theoretical model developed in this paper.

The sample investigated in Ref. 7 consists of a 5-μm ZnSe film epitaxially grown on a (001) GaAs substrate. The HRS experiment was performed in the right-angle scattering geometry, i.e., in $x(yy,0)z$ and $x(zz,0)z$ scattering configurations, where the first, second, and third symbols inside the parentheses refer to the polarizations of the two incident and scattered photons, respectively, ($x\|[100]$, $y\|[010]$, $z\|[001]$, and 0 indicates unpolarized light), and their directions of propagation are indicated outside the parentheses. Figure 4 shows the raw LO-phonon HRS intensities measured by sweeping $2\hbar\omega_L$ through the $2p$ exciton region of ZnSe:[7] Open circles and squares represent the HRS intensities for the $\vec{e}_L\perp z$ and $\vec{e}_L\|z$ scattering configurations, respectively.

The existence of a doublet structure in the HR resonance profile can be traced back to the residual *tensile* in-plane strain present in the ZnSe film due to the mismatch in the thermal expansion of ZnSe and GaAs.[22] Note that this effect has the opposite sign to that expected from the effect of the lattice mismatch in the case of coherent growth (the lattice constant of ZnSe is larger than that of GaAs).[23,24] Coherent (i.e., pseudomorphic) growth, however, is only found in the ZnSe/GaAs system for very thin ZnSe layers ($\lesssim$150 nm). The uniaxial component of the strain associated with the tensile in-plane strain removes the lh-hh valence-band degeneracy, giving rise to two different excitonic transitions, which manifest themselves as distinct peaks in the HR resonance profile (see Fig. 4). Moreover, in Fig. 4 we observe a strong dependence of the resonance profile on the polarization of the incident light. This is due to the fact that the Bloch function symmetries provide different polarization dependence of the scattering process. Let us denote by $|J=\frac{3}{2},J_z=\pm\frac{3}{2}\rangle$ and $|J=\frac{3}{2},J_z=\pm 1/2\rangle$ the Bloch functions of the hh and lh valence bands, respectively. The quantization axis can be taken along the direction of the uniaxial strain, i.e., along [001]. Now we can calculate the polarization selection rules derived from Eq. (21). In the $x(yy,0)z$ scattering configuration we have[25,26]

$$\frac{\mathcal{C}(v_{\rm lh})}{\mu_{\rm lh}}=\sum_{J_z=\pm 1/2}\frac{\mathcal{C}(|J,J_z\rangle)}{\mu_{\rm lh}}=\frac{\sin\theta}{3\mu_{lh}}, \tag{23}$$

$$\frac{\mathcal{C}(v_{\rm hh})}{\mu_{\rm hh}}\sum_{J_z=\pm 3/2}\frac{\mathcal{C}(|J,J_z\rangle)}{\mu_{\rm hh}}=\frac{\sin\theta}{\mu_{\rm hh}}, \tag{24}$$

and, in the $x(zz,0)z$ configuration,

$$\frac{\mathcal{C}(v_{\rm lh})}{\mu_{\rm lh}}=\sum_{J_z=\pm 1/2}\frac{\mathcal{C}(|J,J_z\rangle)}{\mu_{\rm lh}}=\frac{2i\sin\theta}{3\mu_{\rm lh}}, \tag{25}$$

$$\frac{\mathcal{C}(v_{\rm hh})}{\mu_{\rm hh}}\sum_{J_z=\pm 3/2}\frac{\mathcal{C}(|J,J_z\rangle)}{\mu_{\rm hh}}=0, \tag{26}$$

where θ is the angle of the polarization vector of the scattered light with respect to the x axis. The above selection rules clearly show that the $2p$ excitonic transition associated with the heavy-hole band is allowed only for $\vec{e}_L\perp z$, while the transition associated with the light-hole band takes place both for $\vec{e}_L\|z$ and $\vec{e}_L\perp z$. On the other hand, under tensile uniaxial strain the transition from the light-hole ($J_z=\pm\frac{1}{2}$) band to the conduction band shifts to lower energy as compared to that involving the heavy-hole ($J_z=\pm\frac{3}{2}$) band. The experimental results of Fig. 4 are then understood as follows: the two observed peaks come from the $2p$ excitonic resonances associated with lh and hh valence bands, the $2p$(hh) exciton resonance taking place at higher energy than the $2p$(lh) one (from their energy difference, a tensile biaxial strain $\epsilon=4.8\times10^{-4}$ was estimated;[27] the $2p$ exciton energy in unstrained ZnSe is 2.8185 eV).

We have performed calculations of the HR resonance profile within the framework of the model presented in previous sections, in order to check its ability to reproduce the experimental results. The parameters employed are listed in Table I. The hh-lh exciton splitting due to the strain has been fixed according to the experimental data of Ref. 7. The best fit was obtained by using the following values for the exciton broadening: Γ_1(lh)$=0.35$ meV, Γ_1(hh)$=0.45$ meV, and Γ_c(lh) $=\Gamma_c$(lh)$=10$ meV. It is worth mentioning that, in order to simplify the numerical calculations, we have taken an average hole mass $\tilde{m}_{\rm h}=0.24m_0$ for both light and heavy holes. The theoretical calculations are also shown in Fig. 4 as solid and dashed lines: The agreement between calculated and measured values is very good, especially if we take into account that both resonance profiles in Fig. 4 are fitted with the same set of parameters, and the same scale factor is employed in both cases to bring theory and experiment into agreement. The minor discrepancies observed in Fig. 4 chiefly concern the off-resonance range, where our results overestimate the HR efficiency as compared with the experiment. Some disagreement is also apparent in the $2p$(hh) resonance in the $x(yy,0)$ resonance profile, where now the theoretical results are somewhat smaller than the measured ones.

The success in reproducing the key features of the experimental results indicates that the theoretical model elaborated in this paper contains the main ingredients of the nonlinear

hyper-Raman scattering response, and thus can be used, in combination with experimental data, to obtain information on the excitonic structure and the exciton-phonon interaction in semiconductors. In this sense, a good candidate for further RHRS studies would be GaN, a material whose exciton states are known to dominate its optical properties, but are hardly accessible to one-photon laser spectroscopies.[30]

V. CONCLUSIONS

The efficiency of hyper-Raman scattering by LO phonons has been calculated for deformation potential and Fröhlich interaction, taking into account excitonic effects in the framework of the Wannier-Mott exciton model. We conclude that HRS via deformation potential is several orders of magnitude smaller than via Fröhlich interaction, and therefore only the latter case is analyzed in detail.

We show that RHRS allows us to study simultaneously *s* and *p* excitons in cubic crystals. Under resonance conditions $2\hbar\omega_L$ resonates with *p* excitons, whereas the scattered photon $\hbar\omega_S = 2\hbar\omega_L - \hbar\omega_{\mathrm{LO}}$ is resonant with *s*-exciton states (*p* excitons are dipole forbidden). The main feature of the HR resonance profile is that the outgoing peak is much stronger than the incoming one (at least 50 times larger for ZnSe). The calculated HR efficiency reproduces quite well the experimental data available for ZnSe/GaAs thin films. The strain-induced hh-lh energy splitting and its effects on the HR resonance profile are well characterized by the present exciton theoretical model. Improved calculations and experimental measurements of scattering efficiencies should help to decide whether the terms considered in this paper are the only ones of importance in accounting for the experimental resonant HR spectra.

APPENDIX: RADIAL INTEGRAL BETWEEN EXCITON STATES

The matrix element (8) is proportional to

$$P_{\lambda'\to\lambda}(\vec{e}) = \int d^3\vec{r}\,\varphi_\lambda(\vec{r})^*\ \ \vec{e}\cdot\hat{\vec{p}}\,\varphi_{\lambda'}(\vec{r}), \tag{A1}$$

$\hat{\vec{p}} \equiv -i\hbar\vec{\nabla}$ being the linear momentum operator for the relative *e*-*h* motion. Then, for a transition between two exciton states with relative motion energies ΔE_λ and $\Delta E_{\lambda'}$, we have

$$P_{\lambda'\to\lambda}(\vec{e}) = \frac{\mu}{i\hbar}(\Delta E_{\lambda'} - \Delta E_\lambda)\int d^3\vec{r}\,\varphi_\lambda(\vec{r})^*\ \ \vec{e}\cdot\vec{r}\,\varphi_{\lambda'}(\vec{r}). \tag{A2}$$

Moreover, the exciton envelope function can be factorized into angular and radial parts: $\varphi_{\xi,l,m}(\vec{r}) = Y_{l,m}(\Omega)R_{\xi,l}(r)$ (see Refs. 11 and 12 for further details). In the scattering process considered in this paper *m* is always zero, and we need only the matrix element

$$P_{\xi',l'\to\xi,l}(\vec{e}) \equiv P_{\xi',l',0\to\xi,l,0}(\vec{e}) = \frac{\mu}{i\hbar}(\Delta E_{\xi'} - \Delta E_\xi) \times \int_0^{+\infty} r^2 dr \int d\Omega\, R_{\xi,l}(r)Y_{l,0}(\Omega)^* \times \vec{e}\cdot\vec{r}\ \ R_{\xi',l'}(r)Y_{l',0}(\Omega). \tag{A3}$$

The angular integral can be performed resorting to standard properties of the spherical harmonics:[28]

$$P_{\xi',l'\to\xi,l}(\vec{e}) = e_z\frac{\mu}{\hbar}(\Delta E_\xi - \Delta E_{\xi'})\mathcal{R}_{\xi',l'\to\xi,l} \times \left[\sqrt{\frac{(l'+1)^2}{(2l'+1)(2l'+3)}}\,\delta_{l,l'+1} - \sqrt{\frac{l'^2}{(2l'+1)(2l'-1)}}\,\delta_{l,l'-1}\right], \tag{A4}$$

where $\mathcal{R}_{\xi',l'\to\xi,l}$ is

$$\mathcal{R}_{\xi',l'\to\xi,l} = \int_0^\infty r^3 dr\, R_{\xi,l}(r)R_{\xi',l'}(r). \tag{A5}$$

We note that, with the choice of envelope functions made in this paper,[11,12] the matrix elements (A4) are purely real. Also it is apparent that the interaction with the photon field induces a change of ± 1 in the orbital quantum number *l*. Since we are treating the case of an allowed edge, only $l = 0$ excitons participate in the first and last steps of the scattering process shown in Fig. 1, and consequently we need only the matrix elements $P_{\xi',0\to\xi,l}(\vec{e})$:

$$P_{\xi',0\to\xi,l}(\vec{e}) = \delta_{l,1}\frac{e_z}{\sqrt{3}}\frac{\mu}{\hbar}(\Delta E_\xi - \Delta E_{\xi'})\mathcal{R}_{\xi',0\to\xi,l}. \tag{A6}$$

It can be easily shown, following a similar procedure to that employed in Refs. 11 and 12, that the radial integral $\mathcal{R}_{\xi',l'\to\xi,l}$ is given by

$$\mathcal{R}_{\xi',l'\to\xi,l} = a^4 N_{\xi'}\Pi_{\xi',l'}N_\xi\Pi_{\xi,l}\frac{\Gamma(l'+l+4)}{\Lambda^{l'+l+4}} \times F_2\left(l'+l+4, l'+1-\frac{1}{\chi'}, l+1-\frac{1}{\chi}; \times 2(l'+1), 2(l+1); \frac{2\chi'}{\Lambda}, \frac{2\chi}{\Lambda}\right), \tag{A7}$$

where $\Lambda = \chi' + \chi + 0^+$. We recall that $\chi = 1/n$ for the discrete spectrum and $\chi = ik$ for the continuous spectrum (the notations employed can be found in Ref. 11).

*Electronic address: garcial@uv.es

[1] H. Vogt, in *Light Scattering in Solids II*, edited by M. Cardona and G. Guntherödt, Topics in Applied Physics Vol. 50 (Springer, Berlin, 1982), p. 207.

[2] V. N. Denisov, B. N. Mavrin, and V. B. Podobedov, Phys. Rep. **151**, 1 (1987).

[3] K. Inoue, A. Hasegawa, K. Watanabe, H. Yamaguchi, H. Uwe, and T. Sakudo, Phys. Rev. B **38**, 6352 (1988).

[4] W. Richter, in *Solid State Physics*, edited by G. Höhler, Springer Tracts in Modern Physics Vol. 78 (Springer, Berlin, 1976), p. 121; M. Cardona, in *Light Scattering in Solids II* (Ref. 1), p. 19.
[5] K. Watanabe and K. Inoue, J. Phys. Soc. Jpn. **58**, 726 (1989); K. Inoue and K. Watanabe, Phys. Rev. B **39**, 1977 (1989).
[6] K. Watanabe and K. Inoue, Phys. Rev. B **41**, 7957 (1990); K. Watanabe, K. Inoue, and F. Minami, *ibid.* **46**, 2024 (1992).
[7] K. Inoue, K. Yoshida, F. Minami, and Y. Kato, Phys. Rev. B **45**, 8807 (1992); K. Inoue, F. Minami, Y. Kato, and K. Yoshida, J. Cryst. Growth **117**, 738 (1992).
[8] S. Matsushita, F. Minami, K. Yoshida, K. Inoue, and H. Akinaga, J. Lumin. **66-67**, 414 (1996).
[9] Yu. Zavorotnev and L. N. Ovander, Phys. Status Solidi B **68**, 443 (1975).
[10] S. S. Jha and J. W. F. Woo, Nuovo Cimento B **2**, 167 (1971).
[11] A. García-Cristóbal, A. Cantarero, C. Trallero-Giner, and M. Cardona, Phys. Rev. B **49**, 13 430 (1994); A. García-Cristóbal, A. Cantarero, C. Trallero-Giner, and W. Limmer, Phys. Status Solidi B **196**, 443 (1996), and references therein.
[12] A. García-Cristóbal, Ph. D. thesis, University of Valencia, Spain, 1996.
[13] R. J. Elliott, Phys. Rev. **108**, 1384 (1957).
[14] K. C. Rustagi, F. Pradere, and A. Mysyrowitz, Phys. Rev. B **8**, 2721 (1973).
[15] G. D. Mahan, Phys. Rev. **170**, 825 (1968).
[16] Y. Toyozawa, Prog. Theor. Phys. **20**, 53 (1958).
[17] A. K. Ganguly and J. L. Birman, Phys. Rev. **162**, 806 (1967).
[18] G. L. Bir and G. E. Pikus, *Symmetry and Strain-Induced Effects in Semiconductors* (Wiley, New York, 1974).
[19] A. Cantarero, C. Trallero-Giner, and M. Cardona, Phys. Rev. B **39**, 8388 (1989).
[20] C. Trallero-Giner, A. Cantarero, and M. Cardona, Phys. Rev. B **40**, 4030 (1989).
[21] H. Presting and H. Vogt, in *Proceedings of the 17th International Conference on the Physics of Semiconductors*, edited by J. D. Chadi and W. A. Harrison (Springer, New York, 1985), p. 1215.
[22] At low temperatures, the thermal expansion coefficient is positive for GaAs, while it is negative for ZnSe. The reason can be found in the Grüneisen parameters of the TA phonons near the Γ point. [See A. Debernardi and M. Cardona, Phys. Rev. B **54**, 11 305 (1996)].
[23] K. Shahzad, Phys. Rev. B **38**, 8309 (1988).
[24] N. Shibata, Jpn. J. Appl. Phys. **27**, L487 (1989).
[25] F. H. Pollak and M. Cardona, Phys. Rev. **172**, 816 (1968).
[26] C. Trallero-Giner, A. Alexandrou, and M. Cardona, Phys. Rev. B **38**, 10 744 (1988).
[27] F. Minami, Y. Kato, K. Yoshida, K. Inoue, and K. Era, Appl. Phys. Lett. **59**, 712 (1991); **59**, 2057 (1991); J. Cryst. Growth **117**, 565 (1992).
[28] H. A. Bethe and E. E. Salpeter, *Quantum Mechanics of One- and Two-Electron Systems* (Academic, New York, 1957).
[29] *Semiconductors. Intrinsic Properties of Group IV Elements and III-V, II-VI, and II-VII Compounds*, Landolt-Börstein, New Series, Group III, Vol. 22, Pt. a (Springer, Berlin, 1982).
[30] M. Steube, K. Reimann, D. Fröhlich, and S. J. Clarke, Appl. Phys. Lett. **71**, 948 (1997).